ELSEVIER

Applied Ocean Research 21 (1999) 295–309

Applied Ocean Research

www.elsevier.com/locate/apor

On the measurement of directional wave spectra at the southern Brazilian coast

J.H.G.M. Alves[a,*], E. Melo[b]

[a]*School of Mathematics, University of New South Wales, 2052 Sydney, Australia*
[b]*Environmental Engineering Department, Federal University of Santa Catarina, Santa Catarina, Brazil*

Received 4 January 1999; received in revised form 1 July 1999; accepted 9 July 1999

Abstract

The detailed reconstruction of the directional spectrum of wind waves from measurements of the wave field is an essential requirement for several applications, including the numerical modeling of wave evolution. Three reconstruction techniques that provide estimates of the directional distribution function $D(f, \theta)$, given the one-dimensional frequency spectrum, are compared using data from a coastal locality at the southern Brazilian coast. The techniques are the maximum entropy method (MEM), the Fourier Expansion Method using a $\cos^2$ type function (FEM_{cos}) and the Fourier Expansion Method using a sech type function (FEM_{sech}). The main patterns of the wave climate at the study site are qualitatively assessed. Three main sea states, including swell, transition between local sea and swell, and directionally bimodal wind sea, are identified. Time series from three events associated with the main sea states provide test cases for inter comparison of the three reconstruction techniques. Maximum entropy estimates of $D(f, \theta)$ provide results that are more consistent than those obtained from the two FEM techniques in all cases considered.

Keywords: Directional wave spectra; Southern Brazilian coast; Fourier expansion methods; Maximum entropy estimates

1. Introduction

Most present applications of wind wave research for coastal engineering and environmental purposes involve the use of numerical models that simulate the evolution of directional wave energy spectra in time or space or both. Since these models often require the establishment of initial/boundary conditions or validation from observations of the actual wave field, there is an important demand for techniques that allow detailed reconstruction of the directional spectrum from measured data.

Authoritative studies about this topic performed by Donelan et al. [1] and Young [2] have shown that reconstructed directional spectra are significantly affected by the choice of both instrumentation and data analysis techniques. Regarding the use of optimized instrumentation, they give evidence that spatial arrays composed of multiple sensors, arranged in optimal geometrical patterns, can improve considerably the reconstruction of directional spectra from measurements, while the choice of data analysis techniques contributes in a lesser extent to overall improvements.

However, a large number of directional wave observation networks around the world still rely solely on pitch and roll buoys or instruments with similar characteristics. This is particularly true when developing countries are considered. Therefore, meeting the demand of reliable reconstruction of the wind wave spectrum from data collected by such networks resides heavily on the choice of analysis techniques. This is a consequence of the fact that these instruments provide limited information about the directional properties of the wave field.

The present article presents a brief description of the main patterns of the wave climate at a coastal locality at the southern Brazilian coast and compares estimates of directional spreading functions from typical sea states made: (a) through the more traditional and popular Fourier Expansion Method (FEM)—first derived by Longuet-Higgins et al. [3]—and (b) through the maximum entropy method (MEM)—first applied to wind wave spectra by Lygre and Krogstad [4]. The work was motivated by the availability of wave measurements from a recently established network of directional wave-rider buoys along the southern Brazilian coast, and also by the requirements of robust reconstruction techniques for using the measured data as initial and

* Corresponding author. Australian Defence Force Academy, School of Civil Engineering, Canberra, ACT 2600, Australia. Tel.: +61-2-6268 8338; fax: +61-2-6268-8337.

E-mail address: rick@maths.unsw.edu.au (J.H.G.M. Alves)

0141-1187/99/$ - see front matter
PII: S0141-1187(99)00019-X

boundary conditions in numerical wave propagation models in that area [5].

2. General theory

Directional measurements of the wave field made by floating buoys provide the time series

$$X(t) = \{X_1(t), X_2(t), X_3(t)\} \tag{1}$$

where t is time and the subscript "1" refers to the vertical displacement, while "2" and "3" refer to the slopes or displacements in the east and north directions, respectively.

By applying standard cross-spectral analysis to (1), it is possible to obtain nine spectral density functions—three auto-spectra, three co-spectra and three quad-spectra—that can be related back to the frequency-direction wind wave spectrum $E(\omega, \theta)$ through the identities [3]

$$\begin{aligned}
&C_{12}(\omega) = C_{13}(\omega) = Q_{23}(\omega) = 0,\\
&C_{11}(\omega) = \int_0^{2\pi} E(\omega, \theta)\, \mathrm{d}\theta,\\
&C_{22}(\omega) = k^2 \int_0^{2\pi} E(\omega, \theta)\cos^2(\theta)\, \mathrm{d}\theta,\\
&C_{33}(\omega) = k^2 \int_0^{2\pi} E(\omega, \theta)\sin^2(\theta)\, \mathrm{d}\theta,\\
&Q_{12}(\omega) = k \int_0^{2\pi} E(\omega, \theta)\cos(\theta)\, \mathrm{d}\theta,\\
&Q_{13}(\omega) = k \int_0^{2\pi} E(\omega, \theta)\sin(\theta)\, \mathrm{d}\theta,\\
&C_{23}(\omega) = k^2 \int_0^{2\pi} E(\omega, \theta)\sin(\theta)\cos(\theta)\, \mathrm{d}\theta
\end{aligned} \tag{2}$$

where ω is the angular frequency and θ the direction of propagation.

It is more convenient for the present purposes to write $E(\omega, \theta)$ in terms of the one dimensional spectrum $S(\omega)$

$$E(\omega, \theta) = S(\omega)D(\omega, \theta) \tag{3}$$

where $D(\omega, \theta)$ is a directional spreading function satisfying

$$\int_0^{2\pi} D(\omega, \theta)\, \mathrm{d}\theta = 1 \tag{4}$$

To obtain estimates of the full directional spectrum $E(\omega, \theta)$ one must choose analysis techniques capable of providing either the complete directional spectrum itself, as done by Donelan et al. [1] and Young [2], or the one-dimensional spectrum along with its corresponding directional spreading function $D(\omega, \theta)$. (These procedures differ from those used in some engineering applications, where only few characteristic parameters of the directional spectrum, such as the mean direction, the directional width, the skewness and the kurtosis of $D(\omega, \theta)$ at each frequency are determined. For such cases, the reader is referred to Kuik et al. [6]).

The first attempt, by Longuet-Higgins et al. [3] (hereafter LH63), to reconstruct the frequency-direction spectrum from floating buoy measurements consisted of two steps:

1. Obtain the one-dimensional spectrum $S(\omega)$ directly from the auto-spectrum of the vertical displacement $X_1(t)$

$$S(\omega) = C_{11}(\omega) = \frac{1}{2\pi} \int_{-\infty}^{\infty} \overline{X_1(t)X(t+\tau)} e^{-i\omega\tau}\, \mathrm{d}\tau; \tag{5}$$

2. Expand the directional spreading function $D(\omega, \theta)$ as a Fourier series of the form

$$D(\omega, \theta) = \frac{1}{2\pi}\left[1 + \sum_{n=1}^{N} a_n(\omega)\cos n\theta + b_n(\omega)\sin n\theta\right]. \tag{6}$$

If truncated at a finite number N, the series (6) will have a total of $2N$ unknown coefficients a_n, b_n $[n = 1, 2, 3, \ldots, N]$ for a given frequency ω. LH63 [3] shows that only the first four Fourier coefficients a_1, b_1, a_2 and b_2 can be derived from the cross-spectral quantities (2):

$$\begin{aligned}
a_1 &= \int_0^{2\pi} D(\omega, \theta)\cos\theta \mathrm{d}\theta = \frac{Q_{12}}{kC_{11}},\\
b_1 &= \int_0^{2\pi} D(\omega, \theta)\sin\theta\, \mathrm{d}\theta = \frac{Q_{13}}{kC_{11}},\\
a_2 &= \int_0^{2\pi} D(\omega, \theta)\cos 2\theta\, \mathrm{d}\theta = \frac{C_{22} - C_{33}}{k^2 C_{11}},\\
b_2 &= \int_0^{2\pi} D(\omega, \theta)\sin 2\theta\, \mathrm{d}\theta = \frac{2C_{23}}{k^2 C_{11}}
\end{aligned} \tag{7}$$

where the cross-spectral identities (2), the Fourier coefficients and the wave number k are all functions of the frequency ω. Rather than using the wave number obtained theoretically from the linearized dispersion relation, k is estimated directly from the three auto-spectra

$$k = \left\{\frac{C_{22} + C_{33}}{C_{11}}\right\}^{1/2}. \tag{8}$$

Eq. (6) is a truncated Fourier series with $N = 2$. The consequence of the truncation, as discussed by LH63 [3], is the development of negative lobes in the directional spreading function $D(\omega, \theta)$, which should be all positive since both $S(\omega)$ and $E(\omega, \theta)$ are positive definite.

The negative lobes can be avoided by means of the introduction of an appropriate weighting function in the last term of the right-hand side of Eq. (6), as shown by LH63 [3] and Mitsuyasu et al. [7]. Despite providing only positive values for $D(\omega, \theta)$, the weighting function arbitrarily broadens the spreading of the directional distribution. Alternative approaches that avoid this type of problem have been proposed. These approaches may be grouped in two

categories: (i) parametric models based on a priori assumptions about the shape of the spreading functions; and (ii) model free formulations that set no constraints on $D(\omega, \theta)$.

3. Parametric models: the Fourier expansion method

Several authors (e.g. LH63 [3]; Mitsuyasu et al. [7]; Davis and Regier [8]; Hasselmann et al. [9]; Donelan et al. [1]) have proposed analytical forms to approximate the expansion of $D(\omega, \theta)$ as a Fourier series of the form (6). The most widespread—and usually adopted in routine analysis of pitch/roll buoy data—was introduced by LH63 [3] and has the form

$$D(\omega, \theta) = G(s) \cos^{2s}\left(\frac{|\theta - \theta_m(\omega)|}{2}\right) \tag{9}$$

where $G(s)$ is a normalization factor required for satisfying Eq. (4) and θ_m is the mean direction of the energy at frequency ω given by

$$\theta_m = \tan^{-1}\left(\frac{b_1}{a_1}\right) = \tan^{-1}\left(\frac{Q_{13}}{Q_{12}}\right) \tag{10}$$

Although LH63 [3] found that the parameter s controlling the amount of directional spreading is strongly dependent on the relative position of each individual frequency ω to the peak frequency ω_p, the first comprehensive attempt to use instrumental observations to determine the form of s and its frequency dependence was done ten years later by Mitsuyasu et al. [7]. Based on data measured at the coast of Japan with a cloverleaf buoy they parameterized s as

$$s = \begin{cases} s_p\left(\dfrac{\omega}{\omega_p}\right)^{5} & \omega < \omega_p \\ s_p\left(\dfrac{\omega}{\omega_p}\right)^{-2.5} & \omega \geq \omega_p \end{cases} \tag{11}$$

where s_p is the spreading parameter at the peak frequency, defined as a function inversely proportional to the wave age c_p/U_{10}

$$s_p = 11.5\left(\frac{U_{10}}{c_p}\right)^{-2.5} \tag{12}$$

where c_p is the phase speed of waves at the peak of the spectrum and U_{10} a reference wind speed at 10 m height.

The wave age dependence of Mitsuyasu's spreading parameter was questioned by both Hasselmann et al. [9] and Donelan et al. [1]. Hasselmann et al. [9] argued that the dominant process governing the directionality of wind wave spectra is the nonlinear coupling between spectral components of the wave field. Based on data measured at the North Sea during the JONSWAP Project [10], they proposed that the strong dependence of s on the wind input, as expressed by the inverse wave age relation found in Eq. (12), be replaced by a weaker dependence expressed by

$$s = \begin{cases} 6.97\left(\dfrac{\omega}{\omega_p}\right)^{4.06} & \omega < 1.05\omega_p \\ 9.77\left(\dfrac{\omega}{\omega_p}\right)^{\mu} & \omega \geq 1.05\omega_p \end{cases} \tag{13}$$

where μ expresses the dependence of the directional spreading on wave age at frequencies greater than the spectral peak

$$\mu = -2.33 - 1.45\left(\frac{U_{10}}{c_p} - 1.17\right).$$

Recent numerical experiments on the evolution of wind wave spectra support the idea that the amount of spreading of the directional distribution function is almost completely controlled by nonlinear interactions (Young and Van Vledder [11]; Banner and Young [12]). On these grounds, the form (13) can be considered more appropriate than Eq. (11). It is also worth mentioning that Hasselmann et al. used a wider range of wind velocities and stages of spectral evolution—$1.0 < U_{10}/c_p < 1.8$—than Mitsuyasu et al. [7]—$1.0 < U_{10}/c_p < 1.2$, as shown by Young [2].

An alternative form for s which is also consistent with the numerical modeling results cited above is found in Kuik et al. [6]

$$s = \frac{m_1}{1 - m_1} \tag{14}$$

where m_1 is the centered Fourier coefficient defined as

$$m_1 = (a_1^2 + b_1^2)^{1/2}.$$

Besides being independent of properties of the local wind field—as expected if the nonlinear interactions are the dominant directional shaping mechanism—the form (14) is conveniently obtained from the first two Fourier coefficients a_1, b_1 derived directly from the wave field data through the relations (7). It also eliminates the dependence of the spreading parameter s on a single peak frequency found in the other formulations. This last feature introduces a level of independence that is useful when two or more wave fields with energy concentrated at different frequency bands, such as local wind sea and swell, occur simultaneously. For these reasons, the parametric form described above (hereafter referred to as FEM_{cos}) was adopted in the present work.

Considering an extensive data set measured under a broad range of wind velocities and wave spectra conditions—$1.0 < U_{10}/c_p < 2.0$—Donelan et al. [1] (hereafter DHH85 [1]) concluded that the form represented by Eq. (9) was not adequate. Using detailed measurements of the complete wavenumber spectrum obtained with an array of 14 wave staffs at Lake Ontario, Canada, DHH85 [1] arrived at the following alternative parametric form for the directional

spreading function

$$D(\omega, \theta) = 0.5\beta \operatorname{sech}^2 \beta(\theta - \theta(\omega)) \quad (15)$$

DHH85 [1] found that β bore no relation to the wind, but was rather a function of the relative frequency ω/ω_p exclusively, in agreement with the hypothesis that nonlinear coupling between waves determines the shape of the directional spectrum and its evolution. Therefore

$$\beta = \begin{cases} 2.61\left(\dfrac{\omega}{\omega_p}\right)^{1.3} & 0.56 < \dfrac{\omega}{\omega_p} < 0.95 \\ 2.28\left(\dfrac{\omega}{\omega_p}\right)^{-1.3} & 0.95 \le \dfrac{\omega}{\omega_p} < 1.6 \\ 10^{-0.4+0.8393\exp\{-0.567\ \ln[(\omega/\omega_p)^2]\}} & \dfrac{\omega}{\omega_p} \ge 1.6 \end{cases} \quad (16)$$

where the expression for values of $\omega/\omega_p \ge 1.6$ was proposed by Banner [13] after analyzing high frequency stereo photography data.

DHH85 [1], Banner [13] and Young [2] provide sufficient evidence that the parameterization in the form (15) (here after referred to as FEM_{sech}) produces estimates of the directional spectrum that yield a better match to available data and, thus, are more physically reliable than the usual FEM_{cos}. Nevertheless, since the FEM_{cos} are still widely used, both types will be considered for comparison with maximum entropy estimates of the directional distribution obtained from data measured at the southern Brazilian coast.

4. Maximum entropy estimation of $D(\omega, \theta)$

Several model free techniques for the estimation of frequency-direction spectra from measurements have been proposed. In this section we present an overview of recent developments on the subject. For a full account of the available techniques prior to 1992, readers are referred to Tsanis and Brissette [14].

Maximum likelihood (MLM) and maximum entropy (MEM) methods have been considered in the literature as potentially good techniques for this purpose. Lygre and Krogstad [4] (hereafter LK86 [4]) have compared the ability of both MLM and MEM to capture directional spreading functions with known statistical properties from synthetic data. Their results favor MEM estimates since these produce reduced bias for cases with one or two directional peaks, similar to those expected to be found in directionally bimodal wind wave spectra. According to LK86 [4], there was a significantly higher bias in the MLM estimates.

In a similar study, Kobune and Hashimoto [15] (hereafter KH86 [15]) confirm that MEM estimates of the directional distribution are superior to corresponding estimates made with the MLM. Employing a slightly different definition of entropy than that of LK86, their method determines $D(\omega, \theta)$ from a set of Lagrange's multipliers that are computed by solving a set of non-linear functions of the measured Fourier coefficients. The shortcomings of the method are that (1) bimodal directional distributions with peaks separated by less than 60° are not detected; and (2) the solution of the nonlinear equations may diverge, as reported by Kim et al. [16].

Kim et al. [16] employed a set of synthetic directional distribution functions to compare MEM methods proposed by LK86 [4] (MEM-LK) and KH86 [15] (MEM-KH). Their conclusions indicate that (1) MEM-LK has a tendency to overestimate peaks and create false bimodal distributions, while MEM-KH is generally more well behaved in spite of showing a non-convergence problems when measured data from real wave fields are analyzed; (2) both methods are able to describe asymmetric, bimodal directional distributions, while MEM-LK is more suitable for sharp peaked spectra. Kim et al. [16] also propose an approximate method of estimating the Lagrange's multipliers that overcome the MEM-KH non-convergence problem.

Several successful applications of MEM-LK to estimate $D(\omega, \theta)$ from real wave fields have been reported in the literature. Since $D(\omega, \theta)$ in such cases are not known a priori, success is measured indirectly by analyzing jointly the directional properties of the forcing wind field derived from weather charts or meteorological stations and the consistency of the estimated directional distributions. In both cases, a good correspondence between the directional properties of the forcing wind field and the estimated $D(\omega, \theta)$ is observed.

Directional spectra measured with a pitch-and-roll buoy were used by Ewans [17] to assess the performance of MEM-LK. His analysis was concentrated on determining the shape of $D(\omega, \theta)$ within the spectral tail (frequencies higher than twice the peak frequency) where, according to Young et al. [18] $D(\omega, \theta)$ is bimodal. According to Ewans [17], the MEM-LK analysis produced estimates of $D(\omega, \theta)$ that were unimodal around the peak frequency and bimodal, with progressively larger angles of separation between directional peaks, towards higher frequencies. Such results are in agreement with Young et al. [18].

Despite shortcomings related to the generation of spurious bimodal distributions and artificially sharp bimodal peaks when employed to synthetic data, applications of MEM-LK (hereafter MEM) reported in the literature show that it produces satisfactory estimates of $D(\omega, \theta)$ from measurements of real wave fields. In the present work we apply this method to field data and compare results to other two methods widely used in coastal engineering and oceanographic applications. For the sake of completeness, a brief review of the MEM theory is presented in the remaining of this section.

The principle of the MEM is to obtain an estimate of unknown lags of the autocorrelation of a random process, with a spectrum given by some unknown function $f(\theta)$, that maximizes its uncertainty but is, at the same time, consistent

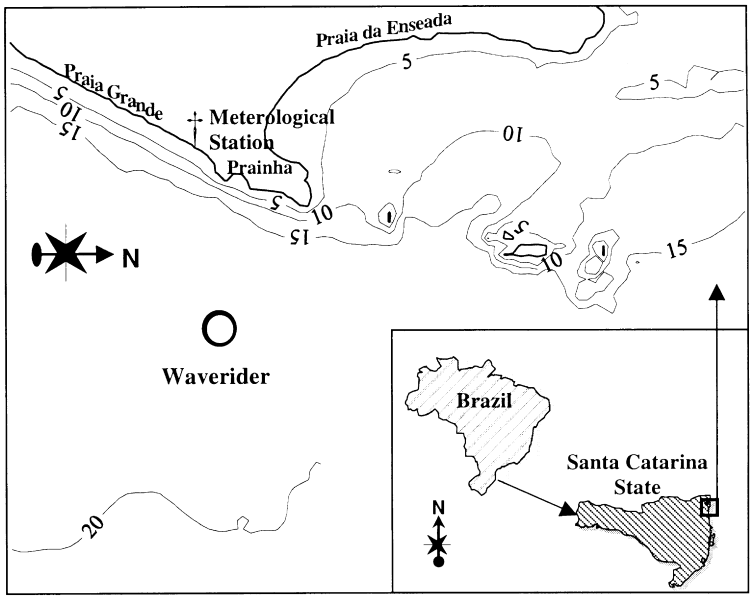

Fig. 1. Location of the study site showing the position of the Waverider buoy and the meteorological station at Praia Grande, Sao Francisco do Sul, state of Santa Catarina.

with known (measured) values of autocorrelation. In accordance with the theory of information (Ulrich and Bishop [19]), the measure of uncertainty of a process is defined, in relation to its spectrum $f(\theta)$, by

$$H(f(\theta)) = -\int_0^{2\pi} \log\left(f(\theta)\right) \mathrm{d}\theta \tag{17}$$

Any form of the unknown spectral function $f(\theta)$ which maximizes H but is still consistent with its known statistical properties should satisfy the constraints

$$\int_0^{2\pi} f(\theta)\, \mathrm{e}^{-\mathrm{i}n\theta}\, \mathrm{d}\theta = c_n \tag{18}$$

where c_n, $[n = 1, 2]$ are the complex Fourier coefficients given by a combination of the identities (7)

$$c_n = a_n + \mathrm{i}b_n \tag{19}$$

It is shown (Ulrich and Bishop [19]) that the function satisfying simultaneously Eqs. (17) and (18) is, using the same notation as LK86 [4], given by

$$f(\theta) = \frac{1}{2\pi}\left[\frac{\sigma_\mathrm{e}^2}{\left|1 - \sum_{n=1}^{N} \phi_n\, \mathrm{e}^{-\mathrm{i}n\theta}\right|^2}\right] \tag{20}$$

Eq. (20) corresponds to fitting a Nth-order auto-regressive (AR) model to the spectrum $f(\theta)$ of the random process at issue (Ulrich and Bishop [19]; Robinson [20]). The parameter σ_e—the variance of the white noise contribution to the AR estimate—is given by

$$\sigma_\mathrm{e} = 1 - \sum_{n=1}^{N} \phi_n c_n^* \tag{21}$$

where c_n^* is the complex conjugate of the correlation coefficient c_n

Now, by recalling that $D(\omega, \theta)$ describes how energy is distributed through all possible directions θ for any given frequency ω (Eq. (4)), $f(\theta)$ may be replaced by $D(\omega, \theta)$ in Eqs. (17)–(21). Therefore, for a second-order AR model, as shown in LK86 [4], the MEM estimate of $D(\omega, \theta)$ is given by

$$D(\omega, \theta) = \frac{1}{2\pi}\left[\frac{1 - \phi_1 c_1^* - \phi_2 c_2^*}{\left|1 - \phi_1\, \mathrm{e}^{-\mathrm{i}\theta} - \phi_2\, \mathrm{e}^{-\mathrm{i}2\theta}\right|^2}\right]. \tag{22}$$

The AR coefficients ϕ_1 and ϕ_2 are obtained after solving the Yule–Walker equations, which, in matrix form, are written as

$$\begin{bmatrix} 1 & c_1^* \\ c_1 & 1 \end{bmatrix}\begin{bmatrix} \phi_1 \\ \phi_2 \end{bmatrix} = \begin{bmatrix} c_1 \\ c_2 \end{bmatrix} \tag{23}$$

and c_n, $[n = 1, 2]$ are obtained from Eq. (19).

5. Wave measurements at the southern Brazilian coast

Measurements of wind wave directional spectra were performed by the Marine Hydrodynamics Laboratory of the Federal University of Santa Catarina at Sao Francisco do Sul, a coastal locality in southern Brazil (Fig. 1) during the year of 1996. The wave measurement campaign was part of a broad environmental monitoring program supported by

Table 1
Wave climate parameters computed from the directional measurement campaign at Sao Francisco do Sul, Brazil. Parameters shown are: mean significant wave height ($\bar{H}_s$), maximum observed significant wave height (H_s^{max}), mean peak period (T_p), maximum observed peak period (T_p^{max}), mean azimuthal main wave direction ($\bar{\theta}_p$), directional range of observed directions (θ_{range}), maximum observed individual wave height (H_{max}) and number of observations per listed period of measurement. Overall and seasonal—Summer (Jan/Feb), Autumn (Mar/Apr/May), Winter (Jun/Aug) and Spring (Sep)—wave climate parameters are presented

Period of measurement	$\bar{H}_s$ (m)	H_s^{max} (m)	T_p (s)	T_p^{max} (s)	$\bar{\theta}_p$ (°)	θ_{range} (°)	H_{max} (m)	Number of observations
All data	1.02	3.44	8.91	16.67	112.42	41.06–174.84	5.59	930
Summer	0.84	1.90	7.71	13.79	102.05	41.06–165.57	3.03	213
Autumn	1.09	3.44	9.18	16.00	115.57	65.38–174.84	5.59	581
Winter	1.10	1.89	9.97	16.67	20.31	71.54–159.49	3.00	88
Spring	0.97	1.27	8.88	15.09	148.06	65.43–148.06	1.98	48

PETROBRAS, the Brazilian Oil Company. The campaign also included observations of sea level, currents and several meteorological parameters.

Wave observations were made with a Datawell Directional Waverider buoy deployed 1.5 km offshore from Praia Grande at a depth of 20 m (Fig. 1). The Waverider buoy is a spherical case of 0.9 m diameter containing an inertia stabilized platform equipped with three accelerometers oriented orthogonally in one vertical and two horizontal directions from which vertical and horizontal (eastward and northward) displacements are obtained. The data is transmitted in real time to a shore-based receiver by means of an on board VHF radio transmitter.

As it is well known, both accelerometer-type and pitch–roll–heave buoys yield essentially the same degree of information about the wave field, which consists of time series of three independent wave related parameters. As pointed out by Tucker [21], accelerometer buoys have the advantage of being cheaper and lighter than pitch–roll–heave buoys, but may produce distorted horizontal displacement measurements due to mooring constraints or strong currents (over 2.5 m s^{-1}). The first effect can be minimized by using a rubber line to connect the instrument to the mooring cable. More detailed performance comparisons of several different wave meters may be found in Krogstad [22] and Allender et al. [23].

Wave observations at Sao Francisco do Sul started on January 1996 and lasted till September 1996, when the Waverider was dragged to the shore during a storm. During this period, 20 min long records were collected eight times a day at three hour intervals. Even though Spring months were not fully represented in the observations, it is believed that the campaign was long enough to identify the main wave patterns expected to exist in the area. In fact, some authors (Taljaard [24], Nimer [25] and Lima and Satyamurti [26]) have pointed out that major meteorological events (calms, frontal systems, storms etc.) occur quite regularly all year round in southern Brazil, regardless of the time of the year. Seasonal differences appear to affect the intensity of these systems rather than their character.

In the next section we present a brief description of the main wave patterns encountered along the southern Brazilian coast. Selected situations are used as test cases for the methodologies described above.

6. Analysis of wave patterns

Alves [5] presents a detailed assessment of the wave conditions encountered at Sao Francisco do Sul whose main characteristics are summarized in Table 1. According to that author, dominant sea states in the area may be grouped as follows: (i) local wind seas, (ii) southeasterly and long traveled swell and (iii) easterly waves.

Representative situations from each one of these three conditions were selected to test the different methods of evaluating $D(\omega, \theta)$ presented previously, namely the maximum entropy method (MEM) and the two Fourier Expansion Methods (FEM_{cos} and FEM_{sech}). All the analysis were performed based on spectral coefficients obtained from smoothed cross spectra calculated from the displacement time series using the Welch method with 32 degrees of freedom and 25% overlap between segments of the time series.

6.1. Local wind sea

Two conditions prevail when locally generated wind seas are considered [5]. These correspond to East–Northeast (ENE) and South–Southeast (SSE) wind seas. ENE seas were mainly observed during summer. Peak periods varied typically from 3 to 8 s, while significant wave heights averaged 0.75 m. Because ENE seas do not contribute significantly to the wave climate's energy budget, they will not be considered further.

Pure SSE wind seas conditions represented approximately 5% of the observations with typical significant wave heights ranging from 1 to 3.5 m and peak periods from 3 to 8 s. SSE seas corresponded to some of the most severe sea states in terms of significant wave heights. This may be explained because of the fact that these conditions are generated by winds associated with low pressure systems carried along the coast by cold fronts, as illustrated by Fig. 2(a). In fact, the passage of cold fronts over southern Brazil is a rather conspicuous feature of the weather in the region all year round. As a consequence, SE swell events are also quite persistent as discussed further ahead.

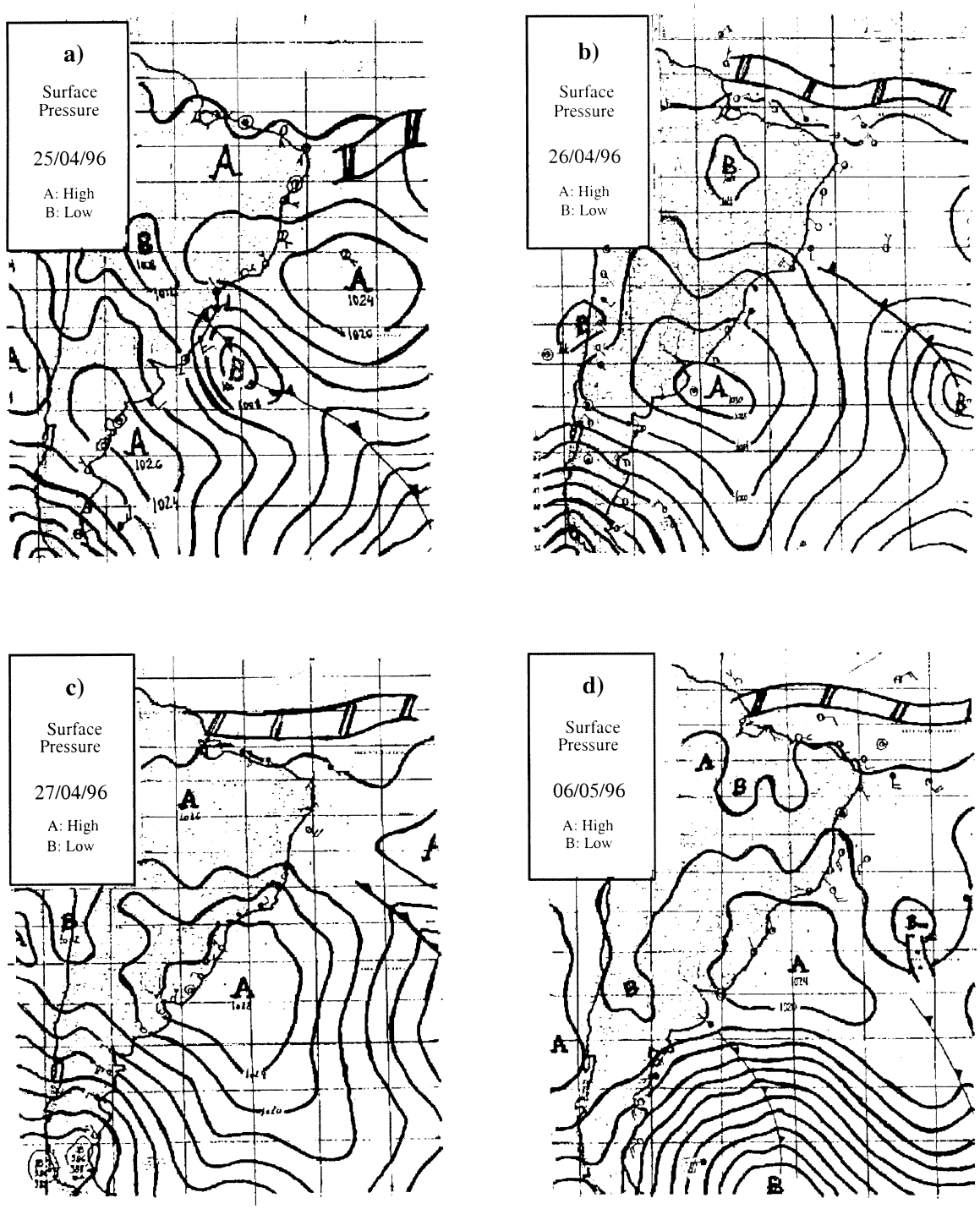

Fig. 2. Surface pressure charts provided by Diretoria de Hidrografia e Navegacao (DHN), Brazilian Navy. The study site is approximately in the middle of each plate. The pressure charts correspond to: (a) the passage of a frontal system (diagonal line with triangles crossing the extra tropical low labeled with the letter "B") over the study site; (b) and (c) a stationary high pressure system (labeled with the letter "A") expanding over the study site; and (d) an extra topical storm centered southeast from the Falkland Islands (the storm is seen as closely spaced isobars forming a semi-circle at the bottom of the figure).

Due to the typical speed of progression of frontal systems and the associated pressure gradients, wind direction and intensity change very quickly within the area. This fact, as will be seen below, results in the generation of a local wave field that has strong two dimensional properties. Therefore, events like these are very convenient test cases for methods that estimate directional properties of the wave field.

Fig. 3(a)–(f) shows the slice of the full two-dimensional spectra taken at the peak frequency at several stages of the evolution of a SSE sea. Fig. 4 shows the full two-dimensional spectrum obtained from the MEM estimate of $D(f, \theta)$.

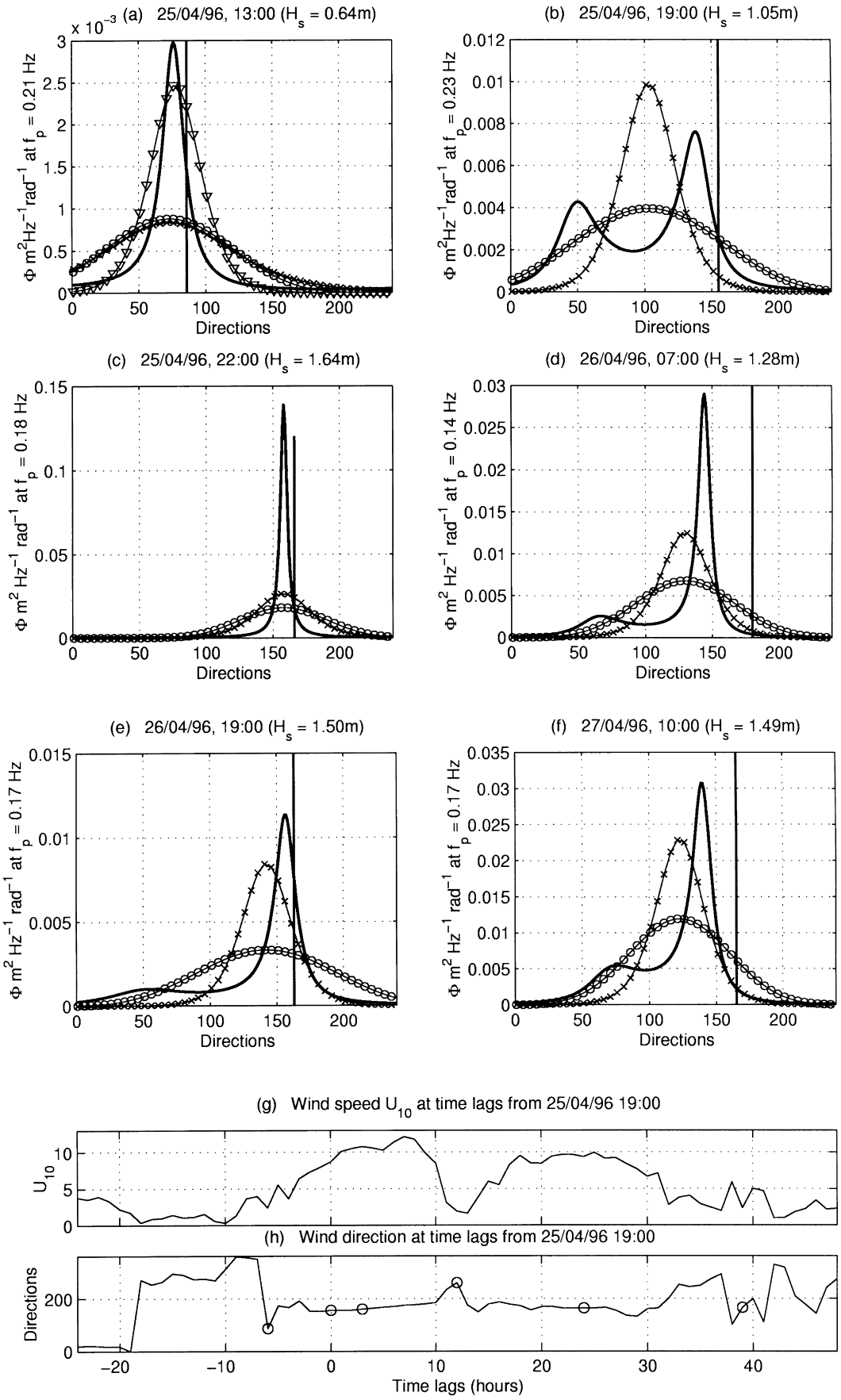
(a) 25/04/96, 13:00 (H_s = 0.64m)
x 10^{-3}
Φ $m^2Hz^{-1}rad^{-1}$ at f_p = 0.21 Hz
Directions
(b) 25/04/96, 19:00 (H_s = 1.05m)
Φ $m^2Hz^{-1}rad^{-1}$ at f_p = 0.23 Hz
Directions
(c) 25/04/96, 22:00 (H_s = 1.64m)
Φ m^2 Hz^{-1} rad^{-1} at f_p = 0.18 Hz
Directions
(d) 26/04/96, 07:00 (H_s = 1.28m)
Φ m^2 Hz^{-1} rad^{-1} at f_p = 0.14 Hz
Directions
(e) 26/04/96, 19:00 (H_s = 1.50m)
Φ m^2 Hz^{-1} rad^{-1} at f_p = 0.17 Hz
Directions
(f) 27/04/96, 10:00 (H_s = 1.49m)
Φ m^2 Hz^{-1} rad^{-1} at f_p = 0.17 Hz
Directions
(g) Wind speed U_{10} at time lags from 25/04/96 19:00
U_{10}
(h) Wind direction at time lags from 25/04/96 19:00
Directions
Time lags (hours)

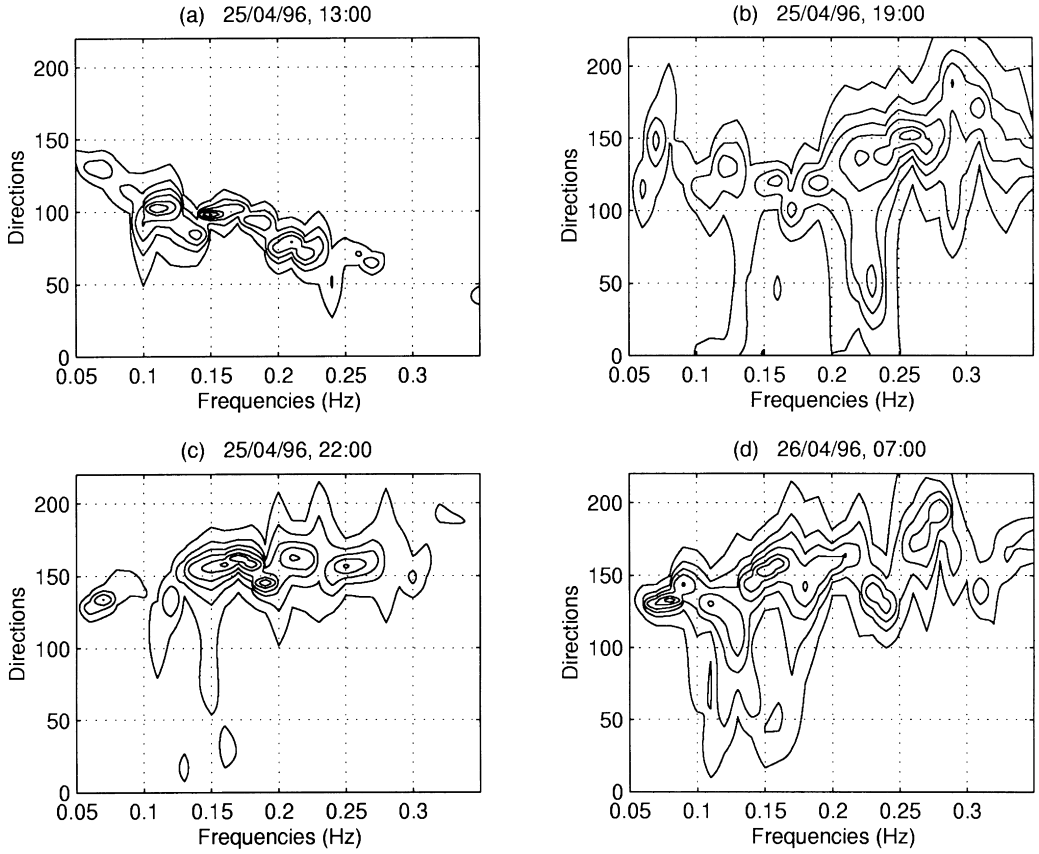

Fig. 4. Two dimensional spectra computed using the maximum entropy method. Items (a)–(d) correspond to the spectra measured at the same time as the corresponding items in Fig. 3.

The three curves in Fig. 3 correspond to the MEM estimate and the two FEM estimates of the directional spreading function $D(f, \theta)$. Fig. 3(g) and (h) illustrates the changes in wind speed and direction associated with the generation of a typical SSE wind sea.

6.2. Easterly waves

Waves arriving from east and southeast dominate the local wave climate [5]. The range of peak periods and significant wave heights expected during easterly wave events are, typically, 6–11 s and 0.5–1.5 m, respectively. The occurrence of easterly waves is usually preceded by the passage of frontal systems. Cold fronts either propagate northward along the coast or steer eastwards towards the Atlantic Ocean, being followed by an anti-cyclone that remains stationary over the study site for several days, producing a lengthy and persistent easterly wind fetch. The development of an easterly sea condition reflects the meteorological history. Initially, the wave field is dominated by easterly wind seas with short peak periods and small wave heights. These progressively evolve to waves that have properties of swell. At this stage, greater periods and heights are likely to be observed.

Fig. 5(a) and (b) shows the evolution of significant wave heights and peak periods for a easterly wave event. Note that the conditions progress gradually from a local wind sea signature, with low values of peak frequency and strong coupling with the local wind speed (Fig. 5(c) and (d)), towards swell conditions, with peak periods well above that expected, considering the local wind speeds. Fig. 2(a)–(c) shows the surface pressure patterns observed during the evolution of such easterly wave events. The corresponding calculated spectral slices in the peak frequency are shown in Fig. 6.

6.3. Southeasterly swell

The majority of calculated spectra associated with south and southeast directions present swell characteristics—

Fig. 3. Evolution of a typical SSE wind sea event. Items (a)–(f) show slices of the two dimensional spectrum illustrating the form of $D(f, \theta)$ estimated by the MEM (thick solid lines), the FEM_{cos} (solid lines with circles) and the FEM_{sech} (solid lines with crosses). The solid vertical lines indicate the wind direction at the time of the measurement. Item (a) also shows an alternative computation of $D(f, \theta)$ by the FEM_{sech} (solid line with inverted triangles). Items (g) and (h) show the evolution of wind speed and direction during the SSE sea event. In (h) the circles correspond to the times in which the spectra in (a)–(f) were measured. Time lags are related to 19:00 of the 25th of April.

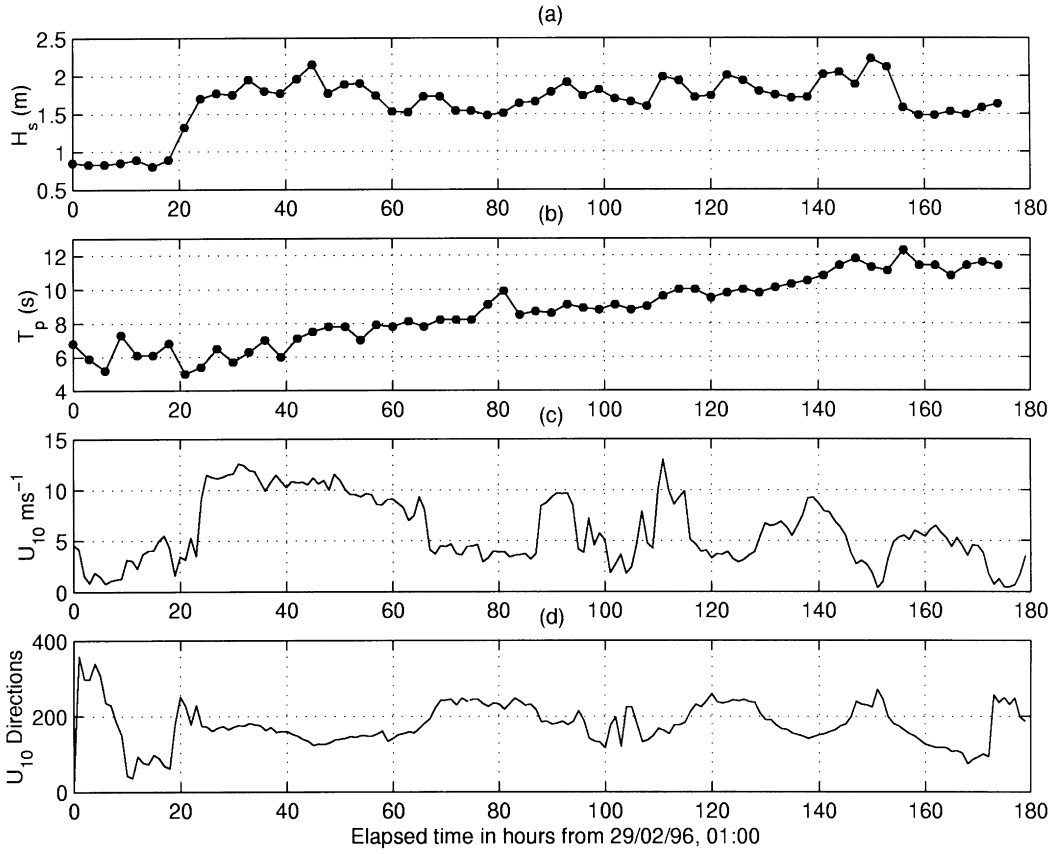

Fig. 5. Evolution of wave and wind parameters during an easterly waves event: (a) significant wave height in meters; (b) peak period of the waves in seconds; (c) wind speed at 10 m height in m s^{-1}; and (d) wind directions. The time lags in hours are relative to 01:00 of the 29th of February.

longer peak periods and no correspondence with the local wind speed or direction. SSE swell is among the most persistent features of the local wave climate [5]. SSE Swell presents peak periods ranging from 7 to 16 s and significant wave heights varying between 1 and 2.5 m.

Two main sources of SSE swell to the Sao Francisco do Sul coast are identified by Alves [5]. The first is associated with paths followed by storms that migrate along the South American coast and deviate towards the ocean within the 20°S and 40°S latitude band. Some of these storms become slow moving systems, allowing the development of persistent southeasterly wind fetches. As they migrate into areas usually dominated by warm air mass systems, these storms develop strong pressure gradients and, consequently, strong wind fields. Distances between the study site and the generation zone may typically be in excess of 1000 km.

The second source generates waves that reach the study site as long traveled swell. They result from storms that, after migrating up the Patagonia coast, in Argentina, deviate to the ocean at latitudes greater than 40°S, where they can become semi-stationary forming south-westerly to south-easterly fetches. Fig. 2(d) shows part of one such storm centered southeast of the Falklands (Malvinas) Islands, off the coast of Argentina. Since the source was more than 4000 km away from the study site, the generated swell was observed at the Sao Francisco do Sul coast over two days after the peak of the storm had occurred.

The distance of the storm shown in Fig. 2(d) was estimated from the progressive decay in wave periods (dispersive arrival) following a very simple methodology [27]. Fig. 7 illustrates the dispersive arrival of the long traveled swell event generated by the storm in Fig. 2(d). The calculated spectral slice at the peak frequency corresponding to the first stages of the event is shown in Fig. 6(d).

The dispersive arrival of long traveled swell is one of the most conspicuous features of wind waves, and it has been reported since the classical contribution of Barber and Ursell [28]. Detailed measurements of the propagation of long traveled swell across the Pacific ocean were first presented by Snodgrass et al. [29]. A similar approach was adopted by Melo and Alves [27] and Melo et al. [30] to confirm the arrival of long traveled Atlantic swell at the southern and northern Brazilian coasts respectively.

7. Discussion

The time history of wind speed and direction shown in Fig. 3(g) and (h) records a steplike change on the 25th of April, a few hours before 19:00 (taken as the reference zero

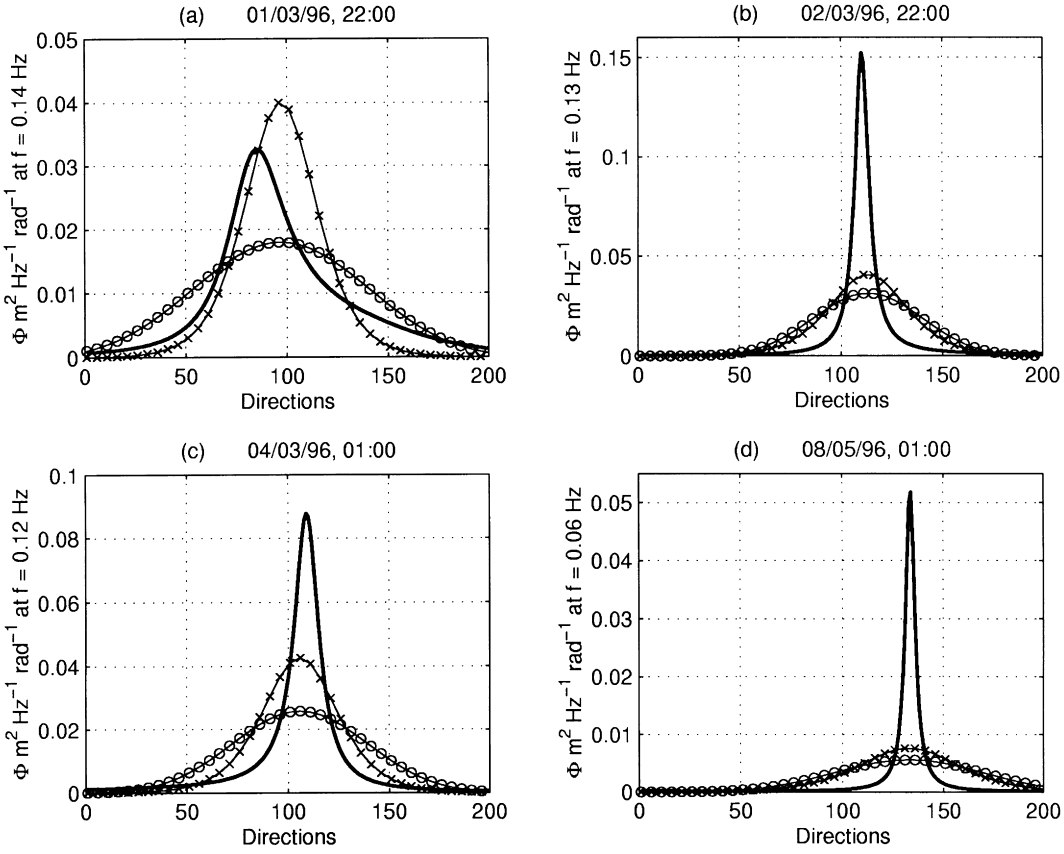

Fig. 6. Slices of the two dimensional spectrum at the peak frequency of: (a) the initial stage of the evolution of a typical easterly waves event; (b) and (c) later stages of evolution of a typical easterly waves event corresponding to swell characteristics; and (d) the arrival of SSE long traveled swell at the study site. The figure illustrates the form of the directional distribution function $D(f, \theta)$ estimated by the MEM (thick solid lines), the FEM_{cos} (solid lines with circles) and the FEM_{sech} (solid lines with crosses).

lag in Fig. 3(g) and (h). The wind speed changes rapidly as the direction swings from North–Northeast to Southwest and finally stabilizes at South–Southeast, corresponding to several stages of the generation of a SSE sea event. A directionally bimodal wave field is expected since, at the time of the wind change, a pre-existing North–Northeasterly wave field is gradually superposed by the SSE seas. Therefore, at the early stages both are expected to coexist and the spectral estimates should be able to identify their joint presence.

As reported in Section 3, the FEM uses only the first two Fourier coefficients to provide one single dominant direction per frequency. Therefore, the FEM will not estimate

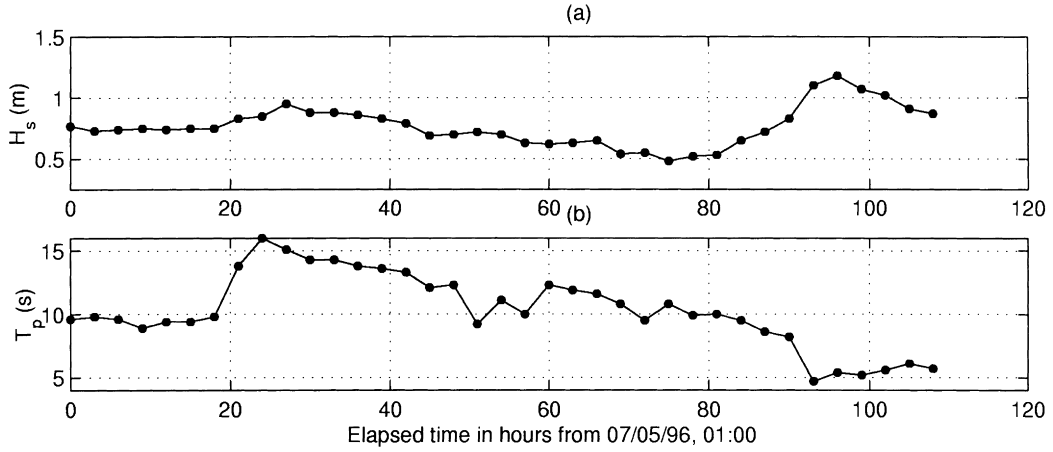

Fig. 7. Evolution of wave parameters during a SSE long traveled swell event: (a) significant wave height in meters; and (b) peak period of the waves in seconds.

properly the directional distribution whenever two or more wave fields with different directions and energy concentrated at similar frequency bands coexist. On the other hand, the MEM estimate should discriminate two dominant directions at the same frequency, for the reasons explained in Section 4. The event shown in Fig. 3 is ideal to test these assumptions. It also allows the identification of other limitations regarding the use of automatic procedures for spectral analysis based on the FEM.

Fig. 3(a) shows the directional distribution $D(f, \theta)$ of energy density $\Phi(f, \theta)$ in mHz rad at the peak frequency of the two-dimensional spectrum corresponding to the measured wave field immediately before the change in wind speed and direction observed on the 25th of April. The full two dimensional spectrum computed using the MEM is shown in Fig. 4(a). The local wind direction is shown in Fig. 3(a)–(f) as a solid vertical line. It is seen that all three estimates of $D(f, \theta)$ indicate the presence of a wave field with dominant direction aligned with the local wind. Even though the overall two-dimensional properties of the spectrum shown in Fig. 3(a) agree qualitatively well, significant differences are found in the shape of $D(f, \theta)$. The differences in shape indicate other limitation from using spectral analysis programs that employ the FEM, as will be pointed out below.

The development of directionally bimodal spectra occurs as a consequence of the steplike change in wind speed and direction observed on the 25th of April. As expected, the differences between FEM and MEM estimates in this case become greater. The first available measurement of the wave field after the change of wind properties was made on the 25th of April at 19:00. The resulting slices of the FEM and MEM spectral estimates at the peak frequency are shown in Fig. 3(b). The full two dimensional spectrum using the MEM estimate of $D(f, \theta)$ is shown in Fig. 4(b).

Both $\mathrm{FEM}_{\cos}$ and $\mathrm{FEM}_{\mathrm{sech}}$ compute a dominant direction that does not correspond either to the newly generated wave field or to the pre-existing waves. On the other hand, the MEM estimate produces a directional spreading function that provides a better match to the expected wave field characteristics. The MEM $D(f, \theta)$ shows both a directional peak in agreement with the local wind direction (solid vertical line) and a secondary directional peak around the pre-existing dominant direction.

The fact that the FEM does not provide consistent estimates of the main direction when directionally bimodal wave fields are present was reported by Kuik et al. [6]. They found that even when the energy of a secondary directional lobe is as small as 20% of that contained in the main lobe, the dominant direction is shifted by as much as 10°. A secondary lobe with 40% of the energy at the main lobe produces shifts as large as 40° (Fig. 4 in Kuik et al. [6]). Their findings are in agreement with what is observed in Fig. 3(b)–(f). The FEM estimates of the main direction are found to be shifted between 10° and 40° from the main directional lobe, depending on the proportion between the energy density at that point and at the secondary lobe.

Fig. 3(c)–(f) shows the remaining stages of the SSE sea event recorded between the 25th and the 27th of April of 1996. The time history of wind speed and direction measured at a meteorological station located near the Waverider buoy position (Fig. 1) is shown in Fig. 3 (items g and h). Circles are assigned to the time at which the spectra shown in Fig. 3(a)–(f) were measured. Fig. 4 shows the full two dimensional spectra with the MEM estimate of $D(f, \theta)$ corresponding to Fig. 3(a)–(d). Note that the two dimensional features in the wave field are present throughout the event, possibly as a result of the persistent changes observed in the wind speed and direction.

A re-examination of Fig. 3(a) reveals that, despite the agreement on the dominant direction of the waves, there is a significant disagreement on the shape of the directional distribution. Both FEM estimates are much broader than the MEM estimate. The reason for this is the presence of two simultaneous wave fields with different characteristics concentrated in different frequency bands. In the full two dimensional MEM spectrum shown in Fig. 4, the local wind sea coupled with the local wind direction is found at frequencies greater than 0.2 Hz, while easterly waves with swell properties are also present at frequencies around 0.1 Hz.

Therefore, two frequency peaks corresponding to easterly waves and SSE sea are present. $\mathrm{FEM}_{\mathrm{sech}}$ uses a single reference peak to calculate the width of the directional spreading (see Eqs. (12), (13) and (16)). As a result, the overall estimate of $D(f, \theta)$ will be systematically biased by the most energetic frequency band, whenever two wave fields centered at different frequency bands are observed simultaneously.

When the procedure outlined in Section 3 is used automatically, the $\mathrm{FEM}_{\mathrm{sech}}$ estimates take the peak frequency of the more energetic wave field, that corresponds to the easterly waves ($f_{\mathrm{p}} = 0.1$ Hz), as the reference f_{p}. The directional distribution obtained this way at the secondary peak, corresponding to the locally generated North–Northeasterly wind sea, is virtually identical for both FEM estimates (lines with circles and crosses in Fig. 3(a)), while the MEM estimate (thick solid line) is significantly narrower. When a second analysis is performed using the secondary peak frequency $f_{\mathrm{p}} = 0.21$ Hz as the reference, the directional spreading obtained using the $\mathrm{FEM}_{\mathrm{sech}}$ (solid line with triangles) is narrower and agrees well with the MEM estimate.

The separation of secondary peaks in measured spectra can be a rather subjective task that would bring further complexities to automatic spectral analysis programs. Neglecting this fact would therefore be a shortcoming inherent to programs that use parametric methods of estimating the directional distribution function, since bimodal seas are frequently observed at the study site and at many other areas with similar atmospheric dynamics. Model free methods such as the MEM do not have such limitation because the

estimate of $D(f, \theta)$ at each individual frequency is independent of the rest of the spectrum and does not depend on a spreading parameter.

In the case of the FEM_{cos} estimate the value of the spreading parameter is independent of the peak frequency. However, it was found that, except in events with strong forcing (very young waves as in Fig. 6(a)), most of the spectra analyzed by Alves [5] had computed spreading parameter s that produced estimates of $D(f, \theta)$ broader than either the MEM or the FEM_{sech} estimates. According to Kuik et al. [6], the broader values of s can be a result of four major factors: noise, errors in the estimation of the wave-number, buoy response and presence of bimodal fields.

Using simulated data, Kuik et al. [6] found that whenever noise is present in one or more of the three buoy signals, there is a rapid increase in the estimated directional width up to 30% of the true value. Small errors in the estimation of the wave-number k can also produce errors in the estimation of s. However, these errors tend to be significant when the theoretical wave-number is used. In the present study, the wavenumber is calculated directly from the spectrum using Eq. (8), as suggested by Kuik et al. [6]. Errors induced by buoy response are also found to be insignificant, around 1% for the most severe case (Kuik et al. [6]). Therefore, it would be expected that the broader estimates of s from FEM_{cos} can be either a result of noise contamination or the presence of directionally bimodal fields or both.

Other possible reason for the broader $D(f, \theta)$ obtained from the FEM_{cos} is pointed out by Donelan et al. [1]. They argue that the information contained in only the first few Fourier coefficients is insufficient to describe narrow directional spectra. Since the spreading parameter is computed from the first two Fourier coefficients of the observed directional energy distribution, it will have a poor performance whenever the directional distribution is expected to be narrower than in strongly forced situations.

Fig. 6(a)–(c) show the slices at the peak frequency of two dimensional spectra corresponding to the evolution of a typical easterly waves event. As described in Section 6, easterly waves evolve initially as locally generated wind seas and progressively assume characteristics usually associated with swell. As argued by Goda [31], directional distribution functions associated with swell conditions should be significantly narrower than those corresponding to local wind seas. Intuitively, this should in fact be expected since the longer distances traveled by swell tend to act as a filter in both the frequency and the directional domains, due to the dispersive nature of wind waves. Furthermore, Alves [5] shows that refraction also narrows significantly the directional spreading of SSE swell.

The FEM parametric forms described in Section 3 were all derived empirically from measurements of wind seas. None of them allow the computation of the potential differences in the directional spreading that exist between local wind seas and swell. Goda [31] presents a set of values for the spreading parameter s based on a steepness parameter that accounts for the expected differences in $D(f, \theta)$ between sea and swell. His approximate values are also based on a widely scattered data set relating s to the wave steepness. For this reason, it is not employed presently.

Fig. 6(a)–(c) shows that the FEM spectra do not produce directional spreading that becomes noticeably narrower as the easterly wave field evolves in time. On the other hand, the MEM estimate seems to reproduce what is expected intuitively. It is possible to assess qualitatively the feasibility of the MEM estimates in the swell stages using the values for the spreading parameter s suggested by Goda [31] for swell with short decay distance ($s = 25$) and long decay distance ($s = 75$). In order to obtain estimates of s from the MEM spectra, a $\cos^{2s}$ type function was fitted to the peak frequency slices of the MEM spectra shown in Fig. 6.

All three estimates of $D(f, \theta)$ in Fig. 6(a) agree well. The computed spreading parameter from FEM_{cos} was $s = 4.54$, while the FEM_{sech} gave $s = 6$ and the MEM gave $s = 5$. This corresponds to a broad directional spreading, typical of actively generated wind seas. Goda [31] reports that the maximum expected value in this case is $s = 20$, which is also in good agreement with the results obtained from the spectral analysis of the data.

Fig. 6(b) and (c) corresponds to a stage where the waves are no longer coupled to the local wind. The wave field, therefore, has the properties of swell. The distance traveled is, however, not very long. According to Goda [31], the expected directional spreading in this case should be approximately $s = 25$. In Fig. 6(b) and (c), FEM_{sech} gives $s = 10.5$ and$s = 8.45$, while FEM_{sech} gives $s = 9$and$s = 10$. All values derived from the FEM estimates still correspond to a directional spreading characteristic of locally generated wind seas. The MEM estimate gives $s = 40$ and $s = 30$, values that agree well with those suggested by Goda.

Fig. 6(d) shows the slice in the peak frequency of a long traveled swell event described in Section 6. The distance of the storm associated with that event was over 4000 km (Fig. 2). It is expected, therefore, that the directional spreading in this case should be narrower than the ones presented above. For long decay distances, Goda [31] suggests a value of $s = 75$. Both FEM estimates, however, produce values of s around 5, while the MEM estimate gives $s = 80$, again in good agreement with both what is expected intuitively and reported by Goda [31].

8. Concluding remarks

Directional wind wave data from a coastal locality at the southern Brazilian coast are used to test three reconstruction techniques of the directional distribution function $D(f, \theta)$. The techniques are employed to obtain estimates of the two-dimensional spectrum for the purpose of numerical modeling of wave evolution. The techniques are the maximum entropy method (MEM) and two other based on the Fourier

expansion method (FEM_{cos} and FEM_{sech}). All three employ lower order Fourier coefficients obtained from cross-spectral analysis of directional data, providing estimates of the directional distribution $D(f, \theta)$ at each frequency of a given one dimensional frequency spectrum.

A qualitative assessment of the main wave climate patterns at the study site is presented, providing three cases that are used to test the performance of the reconstruction techniques. These cases include long traveled swell, transition between local wind sea and swell and directionally bimodal sea generated by veering winds. Spectral analysis of records obtained from events corresponding to the test cases are assessed to provide an inter comparison of the performances of the three reconstruction techniques. The results indicate that:

(a) Directionally bimodal spectra, such as the ones generated by veering winds associated with the passage of frontal systems, are not properly reconstructed by the FEM. By definition, FEM estimates of $D(f, \theta)$ are unable to model more than one directional peak per frequency. When $D(f, \theta)$ is bimodal, FEM estimates produce a single directional peak that lies between the two directional lobes present. As a result, the single FEM directional peak can be significantly shifted from the most energetic directional lobe, not corresponding to either of the wave fields that occur simultaneously. MEM estimates of $D(f, \theta)$ produced two directional lobes consistent with the newly generated wave field and with the pre-existing waves under veering wind conditions.
(b) FEM_{sech} $D(f, \theta)$ are not consistent when two wave fields with energy concentrated in different frequency bands coexist. This is the case when swell and sea are present simultaneously. Whenever the swell is more energetic than the local wind sea, the spreading of $D(f, \theta)$ at the frequency band corresponding to the locally generated waves is systematically overpredicted. The same occurs for FEM_{cos} $D(f, \theta)$ with spreading parameters s that depend on a single peak frequency. This is not the case for *s* obtained as suggested by Kuik et al. [6]. Their spreading parameter, however, produces $D(f, \theta)$ that is too broad when compared with the two other methods, considering the data used presently. Since MEM $D(f, \theta)$ at each frequency are mutually independent and its shape is not determined a priori, the directional spreading is found to produce more reliable results.
(c) MEM and FEM $D(f, \theta)$ agree well when pure unimodal wind seas are present without contamination by swell or pre-existing waves. This is a good indicator of the performance of the MEM under conditions of active wind sea generation because the FEM techniques were formulated to provide the best fit to data measured under such conditions.
(d) Both FEM methods are unable to produce consistent directional distributions of swell with either short or long decay distances. MEM estimates in both cases are consistent with values of directional spreading reported in the literature.

These results indicate that model free techniques such as those based on the maximum entropy method are more suitable and reliable than those based on the FEM whenever the reconstruction of the full directional spectrum is intended.

Acknowledgements

The present study was supported by PETROBRAS and by the Conselho Nacional de Desenvolvimento Cientifico e Tecnologico (CNPq). The authors wish to thank Dr William O'Reilly and Dr Nei Seixas for making available some of the employed spectral analysis codes. We also thank Prof. Ian Young for the encouragement and useful comments on the manuscript.

References

[1] Donelan MA, Hamilton J, Hui WH. Directional spectra of wind generated waves. Phil Trans R Soc London 1985;A315:509–62.
[2] Young IR. On the measurement of directional wave spectra. Appl Ocean Res 1994;16:283–94.
[3] Longuet-Higgins MS, Cartwright DE, Smith ND. Observations of the directional spectrum of sea waves using the motions of a floating buoy. Ocean wave spectra, Englewood Cliffs, NJ: Prentice-Hall, 1963. p. 111–36.
[4] Lygre A, Krogstad HE. Maximum entropy estimation of the directional distribution in ocean wave spectra. J Phys Oceanogr 1986;16:2052–60.
[5] Alves JHGM. Spectral refraction of wind waves in coastal waters: applications to the coastal region of Sao Francisco do Sul, SC. MSc thesis. Federal University of Santa Catarina, Florianopolis, Brazil, 1996, 89 p. (in Portuguese).
[6] Kuik AJ, Van Vledder GP, Holthuijsen LH. A method for routine analysis of pitch-and-roll buoy wave data. J Phys Oceanogr 1988;18:1020–34.
[7] Mitsuyasu H, Tasai F, Suhara T, Mizuno S, Okhuso M, Honda T, Rikiishi K. Observations of the directional spectrum of ocean waves using a cloverleaf buoy. J Phys Oceanogr 1975;5:750–60.
[8] Davis RE, Regier LA. Methods for estimating directional wave spectra from multi-element arrays. J Marine Res 1977;35:453–77.
[9] Hasselmann DE, Dunckel M, Ewing JA. Directional wave spectra observed during JONSWAP. J Phys Oceanogr 1980;10:1264–80.
[10] Hasselmann K, et al. Measurements of wind-wave growth and swell decay during the Joint North Sea Wave Project (JONSWAP). Dtsch Hydrogh Z (Suppl A) 1973;8(12):95.
[11] Young IR, Van Vledder GP. A review of the central role of nonlinear interactions in wind-wave evolution. Phil Trans R Soc London 1993;342:505–24.
[12] Banner ML, Young IR. Modeling spectral dissipation in the evolution of wind waves. Part I: Assessment of existing model performance. J Phys Oceanogr 1994;24:1550–71.
[13] Banner ML. Equilibrium spectra of wind waves. J Phys Oceanogr 1990;20:966–84.
[14] Tsanis IK, Brissette FP. Methods for directional spectra measurements by small arrays. Third International Workshop on Wave Hindcasting and Forecasting, Montreal, 1992. p. 12–23.
[15] Kobune K, Hashimoto N. Estimation of directional spectra from the maximum entropy principle, Proceedings of the Fifth International

Offshore Mechanics and Arctic Engineering Symposium, Tokyo, Japan, 1 1986. p. 80–5.
[16] Kim T, Lin L, Wang H. Comparisons of directional wave analysis methods, Proceedings of the Second International Symposium on Ocean Wave Measurement and Analysis, New Orleans, USA 1993. p. 554–68.
[17] Ewans KC. Observations of the directional spectrum of fetch-limited waves. J Phys Oceanogr 1998;28:495–512.
[18] Young IR, Verhagen LA, Banner ML. A note on the bimodal directional spreading of fetch-limited wind waves. J Geophys Res 1995;100(C1):773–8.
[19] Ulrich TJ, Bishop TN. Maximum entropy spectral analysis and autoregressive decomposition. Rev Geophy Space Phys 1975;13:183–200.
[20] Robinson EA. Physical applications of stationary time-series, London: Griffin, 1980. p. 302.
[21] Tucker MJ. Waves in ocean engineering: measurement, analysis, interpretation, Ellis Horwood Series in Marine Sciences. London: Ellis Horwood, 1991. p. 431.
[22] Krogstad HE. Reliability and resolution of directional wave spectra from heave, pitch and roll buoy wave data. In: Beal RC, editor. Directional ocean wave spectra, Baltimore, MD: The Johns Hopkins University Press, 1991. p. 66–71.
[23] Allender J, Audunson T, Barstow SF, Bjerken S, Krogstad HE, Steinbakke P, Vartdal L, Borgman L, Graham C. The WADIC Project: a comprehensive field evaluation of directional wave instrumentation. Ocean Engng 1989;16:505–36.
[24] Taljaard JJ. Development, distribution and movement of cyclones and anticyclones in the Southern Hemisphere during the IGY. J Appl Meteor 1967;6(6):973–87.
[25] Nimer E. Climatology of Brazil. IBGE, Dept. Recursos Naturais e Estudos Ambientais, Rio de Janeiro, 1989. p. 421 (in Portuguese).
[26] Lima LCE, Satyamurti P. An observational study of formation and trajectories of extratropical anticyclones in South America. Proceedings of VII Congress of Brasilian Meteorologists, 2, 1992. p. 706–10.
[27] Melo E, Alves JHGM. A note on the arrival of long traveled swell at the Brazilian coast. Proceedings of the X Simp Bras Rec Hidricos, ABRH, Gramado, RS, 5, 1993. p. 362–9 (in Portuguese).
[28] Barber NF, Ursell F. The generation and propagation of ocean waves and swell. Phil Trans R Soc London 1948;A240:527–60.
[29] Snodgrass FE, Groves GW, Hasselmann KF, Miller GR, Munk WH, Powers WM. Propagation of swell across the Pacific. Phil Trans R Soc London 1966;A259:431–97.
[30] Melo E, et al. Instrumental confirmation of the arrival of North Atlantic swell to the Ceara coast, Proceedings of the 4th International Conference on Coastal and Port Engineering in Developing Countries. COPEDEC IV, Rio de Janeiro, Brazil, 1995;3:1984–96.
[31] Goda Y. Random seas and design of maritime structures, Tokyo: University of Tokyo Press, 1977. p. 323.